

# A complete view of the broad-line radio galaxy 4C+74.26 with *XMM-Newton*

D. R. Ballantyne <sup>\*</sup>

*Canadian Institute for Theoretical Astrophysics, 60 St. George Street, Toronto, Ontario, Canada M5S 3H8*

24 June 2018

## ABSTRACT

This paper presents a timing study and broadband spectral analysis of the broad-line radio galaxy 4C+74.26 based on a 35 ks *XMM-Newton* observation. As found in previous datasets, the source exhibits no evidence for rapid variability, and its 0.2–10 keV lightcurve is well fit by a constant. An excellent fit to the pn 0.3–12 keV spectrum was found using a continuum that combines an ionized and a neutral reflector, augmented by both cold and warm absorption. There is no evidence for a soft excess. The column of cold absorption was greater than the Galactic value with an intrinsic column of  $\sim 1.9 \times 10^{21} \text{ cm}^{-2}$ . Evidence for the warm absorber was found from O VII and O VIII absorption edges with maximum optical depths of  $\tau_{\text{O VII}}^{\text{max}} = 0.3$  and  $\tau_{\text{O VIII}}^{\text{max}} = 0.03$ , respectively. A joint pn-MOS fit increased the O VIII optical depth to  $\tau_{\text{O VIII}}^{\text{max}} = 0.1$ . A simple, one-zone warm absorber model yielded a column of  $\sim 9 \times 10^{20} \text{ cm}^{-2}$  and an ionization parameter of  $\sim 60$ . Partial covering models provide significantly worse fits than ones including a relativistically broadened Fe K $\alpha$  line, strengthening the case for the existence of such a line. On the whole, the X-ray spectrum of 4C+74.26 exhibits many features typical of both a radio-loud quasar (excess absorption) and radio-quiet Seyfert 1 galaxies (Fe K $\alpha$  emission and warm absorption). We also show that a spurious absorption line at  $\sim 8 \text{ keV}$  can be created by the subtraction of an instrumental Cu K $\alpha$  emission line.

**Key words:** galaxies: active — galaxies: individual: 4C+74.26 — X-rays: galaxies

## 1 INTRODUCTION

4C+74.26 ( $z = 0.104$ ; Riley et al. 1988) is a luminous broad-line radio galaxy (BLRG) most notable for its large radio lobes, extending 10 arcminutes (tip-to-tip) on the sky (Riley et al. 1988). A one-sided jet has been observed with the VLA (Riley & Warner 1990) and on pc scales with VLBI (Pearson et al. 1992). The flux limit on a counterjet gives a limit to the inclination angle of  $i \lesssim 49$  degrees (Pearson et al. 1992), resulting in a physical size for the radio source of  $\sim 2 \text{ Mpc}$  (using a *WMAP* cosmology:  $H_0 = 70 \text{ km s}^{-1} \text{ Mpc}^{-1}$ ,  $\Omega_\Lambda = 0.73$ ,  $\Omega_0 = 1$ ; Spergel et al. 2003), well within the range to be classified as a giant radio galaxy (Lara et al. 2001, 2004). The observed morphology of the radio jets clearly places it as a FRII source, although the radio luminosity of 4C+74.26 is on the border between FRI and FRII (Riley et al. 1988). The bolometric luminosity has been estimated to be  $L_{\text{bol}} \approx 2 \times 10^{46} \text{ ergs s}^{-1}$  (Woo & Urry 2002), indicating that 4C+74.26 is also close to the Seyfert-quasar border. The host galaxy has a size and luminosity typical of other giant ellipticals associated with radio sources (Riley et al. 1988). Optical spectra reveal very broad permitted lines with measurements of the H $\beta$  FWHM ranging from  $\sim 8000 \text{ km s}^{-1}$  (Riley et al. 1988; Brinkmann et al. 1998; Robinson et al. 1999) to  $11,000 \text{ km s}^{-1}$

(Corbin 1997). Using this last value, Woo & Urry (2002) employ the broad-line region radius-luminosity relation (Kaspi et al. 2000) to obtain a black hole mass of  $\sim 4 \times 10^9 M_\odot$ .

X-ray observations of 4C+74.26 began with a 23 ks *ASCA* observation in 1996. Brinkmann et al. (1998) presented the first analysis of these data, as well as *ROSAT* data. The data from the *ROSAT* All-Sky Survey yielded a very hard photon-index for the 0.3–2 keV band,  $\Gamma = 1.2 - 1.3$ , with a cold absorption column slightly above the Galactic value of  $1.19 \times 10^{21} \text{ cm}^{-2}$  (Dickey & Lockman 1990). *ROSAT* PSPC data of 4C+74.26 was available from a 20 ks observation of the cataclysmic variable VW Cep during which the BLRG was in the field-of-view. An absorbed power-law fit to this dataset by Brinkmann et al. (1998) also revealed a hard power-law ( $\Gamma \sim 1.6$ ) with higher than Galactic absorption. A later analysis of this PSPC data by Komossa & Meerschweinchen (2000) found that a dusty warm absorber model provided a good fit and increased the photon-index to values closer to those found in the *ASCA* data ( $\Gamma \approx 2$ ) and in *ROSAT* samples of radio-loud quasars (e.g. Brinkmann, Yuan & Siebert 1997).

The *ASCA* data has subsequently been re-analyzed by Sambruna, Eracleous & Mushotzky (1999) and Reeves & Turner (2000). All groups found a best fit model that included a power-law with a photon index  $\Gamma \approx 2$  and cold absorption in excess of the Galactic value. However, Brinkmann et al. (1998) preferred a solution with a warm absorber, while the best fit of

\* ballantyne@cita.utoronto.ca

Sambruna et al. (1999) did not require one ( $\tau_{\text{O VII}} < 0.8$ ). Similarly, Brinkmann et al. (1998) and Reeves & Turner (2000) find a Gaussian Fe K $\alpha$  line at the 97 per cent confidence level, but Sambruna et al. (1999) find one about twice as strong and at  $> 99$  per cent confidence. The *ASCA* data also show a hardening at high energies, which Brinkmann et al. (1998) and Reeves & Turner (2000) model with a reflection continuum, but find very high reflection fractions ( $R \sim 6$  and  $3$ , respectively). Sambruna et al. (1999) argue that such a large reflection fraction should yield a much stronger Fe K $\alpha$  line, and propose a model where the hardening is due to a second, very hard power-law with  $\Gamma \sim 0.2$ , possibly arising from the radio jet.

This confusing situation was improved by a 100 ks *BeppoSAX* observation presented by Hasenkopf, Sambruna & Eracleous (2002). No significant variability was detected from 4C+74.26 even in the high-energy PDS band. This fact provides strong evidence that jet emission is not significantly contributing to the hard X-rays. Indeed, Hasenkopf et al. (2002) find that Compton reflection provides the best fit to their broadband data with  $R \sim 1$ . These authors also find cold absorption in excess of the Galactic value, but a warm absorber is not required by the data. A significant, but unresolved, Fe K $\alpha$  line was also detected in the *BeppoSAX* spectrum.

More recently, very preliminary results from a 70 ks *Chandra* gratings observation of 4C+74.26 have been presented by Kaspi (2004). A highly ionized and weak warm absorber was detected by *Chandra*, including emission and absorption lines from H-like and He-like Mg, Al and Si. Moreover, the low number of counts at energies less than 0.8 keV could indicate O VII and O VIII edges (Kaspi, private communication).

Here, we present the results of a 35 ks *XMM-Newton* observation of 4C+74.26 which will for the first time properly characterize the X-ray spectrum of this source. The detection of a relativistically broadened Fe K $\alpha$  line has already been reported elsewhere (Ballantyne & Fabian 2005; hereafter Paper I). This paper therefore concentrates on the timing analysis (Sect. 3) and fitting the broadband spectrum (Sect. 4). The paper concludes by discussing the results in Sect. 5. We begin in the next section by describing the details of the observation and data reduction.

## 2 OBSERVATIONS AND DATA REDUCTION

4C+74.26 was observed by *XMM-Newton* (Jansen et al. 2001) for 35 ks during revolution 762 starting at 2004 February 6 13:57:42. Data were collected using the single pn (Strüder et al. 2001) and two MOS (Turner et al. 2001) detectors in the European Photon Imaging Camera (EPIC) system, both Reflection Grating Spectrometers (RGS; den Herder et al. 2001) and the Optical Monitor (OM; Mason et al. 2001). The EPIC instruments were operated in large-window mode with the medium optical filter in place. The RGS was operated in standard spectroscopy mode.

Data reduction was performed using the *XMM-Newton* Science Analysis System (SAS) v.6.1. The analysis chains EPCHAIN and EMCHAIN were run on the observation data files to produce calibrated event lists for the MOS and pn detectors by removing bad pixels and applying both gain and Charge Transfer Inefficiency (CTI) corrections to the data<sup>1</sup>. Source spectra were extracted using circles of radius 115 arcseconds (for the pn), 119 arcseconds

(MOS1) and 122 arcseconds (MOS2). Background spectra were extracted from source free areas on the same CCD using circles with radii of 60 arcseconds (pn and MOS1) and 50 arcseconds (MOS2). The extracted pn spectrum included both single and double events, while the MOS spectra were comprised of events with all patterns. The background was negligible during the observation except for a minor enhancement at  $\sim 22$  ks into the integration. A good-time interval file was constructed as described in § 4.4.3 of the *XMM-Newton* SAS User's Guide<sup>2</sup> to remove any potential contamination by background events. The SAS task EPATPLOT was used to check the pattern distributions in the EPIC data, and both MOS spectra were found to suffer from a non-negligible amount of pileup (Ballet 1999). To correct this, the MOS spectra were re-extracted using only single (i.e., pattern 0) events. Following background subtraction, the final pn spectrum has 28.8 ks of good exposure time and consists of over  $2.5 \times 10^5$  counts, giving a mean count rate of  $8.6 \text{ s}^{-1}$ . The final background subtracted MOS-1 and MOS-2 spectra each had mean count rates of  $2.2 \text{ s}^{-1}$ , and contained  $7.4 \times 10^4$  and  $7.5 \times 10^4$  counts, respectively. Prior to spectral analysis, all data were grouped using GRPPHA to have a minimum of 20 counts per bin. Finally, the SAS tasks RMFGEN and ARFGEN were utilized to produce the response matrix and ancillary response files.

We note that the background extraction regions used above are smaller than the source extraction regions. This was done in order that the background was taken from either the same CCD or same window as the majority of the source counts. To check the spectral analysis described in the following section, larger background regions from a different CCD with radii equal to or larger than the source regions were also extracted. The derived spectral parameters were not significantly changed by using the larger background regions, therefore we report the results from the original data extraction.

The RGS data were reduced using the RGSPROC chain in the SAS. The observed count rate was  $0.15 \text{ s}^{-1}$  for RGS1 and  $0.19 \text{ s}^{-1}$  for RGS2. This yielded only  $5.6 \times 10^3$  and  $6.8 \times 10^3$  counts in the RGS1 and RGS2 spectra, respectively. Given the small number of counts it was decided not to pursue a detailed analysis of the RGS spectra, although the continua predicted by the broadband pn models (including the warm absorption edges) were checked against the observed RGS spectral shape.

## 3 TIMING ANALYSIS

Figure 1 shows the 0.2–10 keV pn lightcurve of 4C+74.26 in 100 s time bins. The SAS task LCCORR was used to background subtract the data, as well as provide corrections for vignetting and deadtime. As with the earlier *ASCA* (Brinkmann et al. 1998) and *BeppoSAX* (Hasenkopf et al. 2002) observations, no significant variability was observed from 4C+74.26. A constant fit to the pn lightcurve resulted in a  $\chi^2/\text{d.o.f.} = 267/317$  (d.o.f.=degrees of freedom), with a best fit of  $8.57 \text{ s}^{-1}$ .

## 4 SPECTRAL ANALYSIS

In this section we present the results of fitting the *XMM-Newton* spectrum of 4C+74.26 between 0.3 and 12 keV in the observed

<sup>1</sup> see, e.g., <http://xmm.vilspa.esa.es/sas/current/doc/epchain/index.html>

<sup>2</sup> [http://xmm.vilspa.esa.es/external/xmm\\_user\\_support/documentation/sas.usg\\_3.0/USG/USG.html](http://xmm.vilspa.esa.es/external/xmm_user_support/documentation/sas.usg_3.0/USG/USG.html)

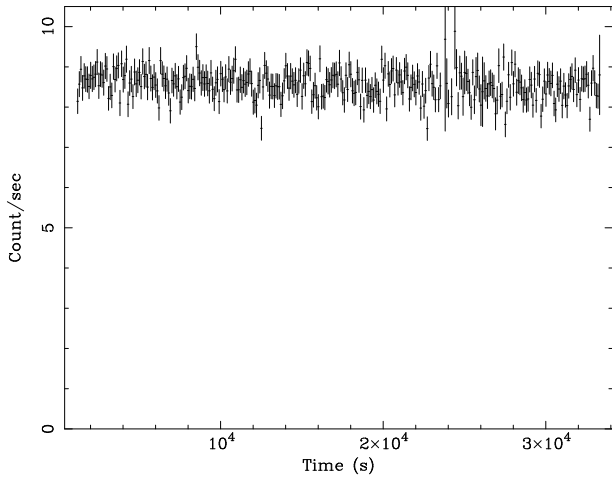


**Figure 1.** The 0.2–10 keV pn lightcurve of 4C+74.26 plotted using 100 s time bins. The data were background subtracted and corrected for vignetting and deadtime losses.

frame. Since it has the largest number of counts and higher spectral resolution, the pn spectrum was initially analyzed on its own, but we include the MOS data (from 0.3–10 keV) at the end of this section to check for any differences. As mentioned above, results for the Fe  $K\alpha$  line region and reflection parameters are presented in Paper I. Here, we will concentrate on the absorption characteristics in the observed spectrum. XSPEC v.11.3.1p (Arnaud 1996) was used for the spectral fitting, and a  $\Delta\chi^2 = 2.71$  criterion was used to determine the  $2\sigma$  errorbars on the best-fit parameters. Galactic absorption, modeled using the 'TBabs' code in XSPEC (Wilms, Allen & McCray 2000), is included in all fits. Unless stated otherwise, the figures are plotted in the observed frame, while the fit parameters are quoted in the rest frame.

We begin the analysis with the best-fitting model found in fitting the 2–12 keV data. This model, denoted IONDISK\*blr+IONDISK+G in Paper I, consists of a relativistically blurred ionized disk (employing the models of Ross, Fabian & Young 1999), an unblurred neutral reflector (also using the Ross et al. 1999 models), and a narrow Gaussian emission line. The data-to-model ratio when the 0.3–2 keV data are included is shown in Figure 2. The plot clearly shows that a significant amount of absorption is required at energies  $< 2$  keV. This opacity could be in the form of extra cold absorption (as favored by the earlier analyses of Sambruna et al. 1999 and Hasenkopf et al. 2002), warm absorption (as indicated by Kaspi 2004), or a combination of the two.

To test the different absorption models, we first froze the parameters in the model related to the Fe  $K\alpha$  lines, and then added additional intrinsic absorption via the 'ztbabs' model in XSPEC. A good fit was found ( $\chi^2/\text{d.o.f.}=1643/1643$ ) to the 0.3–12 keV spectrum with an intrinsic column  $N_{\text{H}}^{\text{intr}} = 1.83 \times 10^{21} \text{ cm}^{-2}$ . When the cold absorption model was replaced with the warm absorber model 'absori' (Done et al. 1992), the ionization parameter of the absorber went to zero and basically the same fit was uncovered as before ( $\chi^2/\text{d.o.f.}=1638/1642$ ). However, the *Chandra* data of 4C+74.26 show evidence for a weak warm absorber with possible ionized oxygen edges. To check this, an O VIII edge at 0.87 keV and an O VII edge at 0.739 keV were added to the cold absorption model above. This new model resulted in a significant ( $\Delta\chi^2 = -54$  with only 2 additional degrees of freedom) improvement over the purely cold absorber case, bolstering the case for a

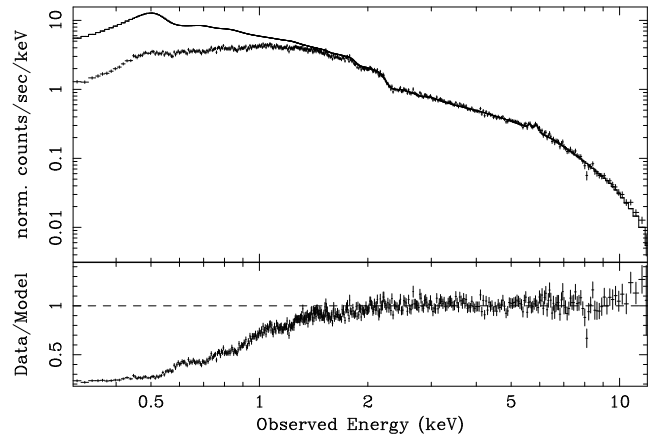


**Figure 2.** The top panel shows the pn count spectrum of 4C+74.26, while the lower panel displays the data-to-model ratio between 0.3 and 12 keV when the model (solid line in the top panel) IONDISK\*blr+IONDISK+G from Paper I is extended to low energies. Significant absorption is required at energies below 2 keV.

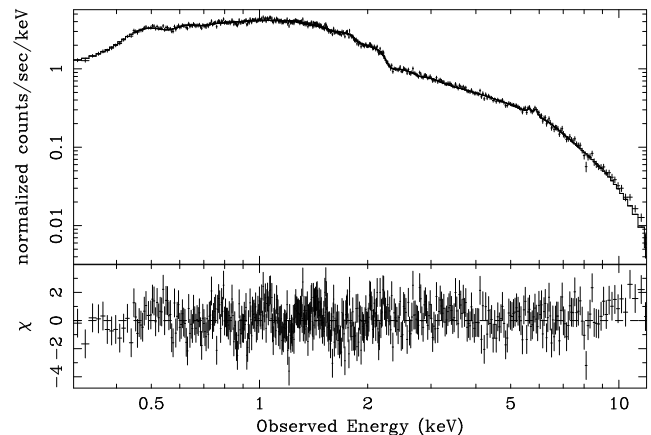


**Figure 3.** The top panel shows the pn count spectrum of 4C+74.26 with the solid line denoting our best fit model (2nd line in Table 1). The residuals to the fit in units of standard deviations are shown in the lower panel. There is no evidence for a soft excess.

warm absorber toward 4C+74.26. Since the previous model excluding the warm absorber resulted in a statistically acceptable fit, it is not possible to conclude that the data require warm absorption. The results of the fit are shown in the first line of Table 1. There is strong evidence for an O VII edge in the data with a maximum optical depth of  $\sim 0.2$ – $0.3$ , consistent with the limit from the *ASCA* data. A further improvement to the fit was made when the Fe  $K\alpha$  line parameters were allowed to vary (second line in Table 1). Except for  $\tau_{\text{O VII}}^{\text{max}}$ , the absorption parameters did not change significantly. The residuals to this last fit (our best-fit model) are shown in Figure 3, while the model is displayed in Figure 4.

The residuals show no evidence for a soft excess. The neutral reflector predicts soft X-ray emission lines from O VII and O VIII that do seem to be accounted for in the data. It would be interesting to obtain a long gratings observation with either *XMM-Newton* or *Chandra* to confirm this possibility.

The above fits give strong indications that a warm absorber is present in 4C+74.26, but unfortunately cannot give much further information. In order to try to further characterize the warm absorber, we performed a fit where we replaced the absorption edges with the

**Table 1.** Results from fitting the spectrum of 4C+74.26 from 0.3 to 12 keV. The spectral model includes two absorption edges fixed at the energies of O VII and O VIII (0.739 keV and 0.87 keV, respectively), intrinsic cold absorption, Galactic absorption, and the double reflector plus Gaussian model from Paper I. In the first line of the table, the parameters affecting the Fe K $\alpha$  line were frozen at their best fit values from Paper I. The final row presents the results from a joint pn-MOS fit, where the MOS data were used between 0.3 and 10 keV. In this case, only the photon-index from the pn data is reported.  $\Gamma$  is the photon-index of the incident power-law,  $N_{\text{H}}^{\text{intr}}$  is the column of the intrinsic cold absorber ( $\text{cm}^{-2}$ ),  $\xi$  is the ionization parameter of the ionized reflector which makes up most of the continuum,  $\tau_{\text{O VIII}}^{\text{max}}$  and  $\tau_{\text{O VII}}^{\text{max}}$  are the maximum optical depths in the O VIII and O VII edges respectively,  $r_{\text{out}}$  is the outer radius of the blurred ionized reflector (gravitational radii),  $i$  is the inclination angle (degrees), and  $E$  is the energy of the narrow Gaussian emission line (keV).

$\Gamma$	$N_{\text{H}}^{\text{intr}}$	$\log \xi$	$\tau_{\text{O VIII}}^{\text{max}}$	$\tau_{\text{O VII}}^{\text{max}}$	$r_{\text{out}}$	$i$	$E$	$\chi^2/\text{d.o.f.}$
$1.86 \pm 0.01$	$(1.87 \pm 0.05) \times 10^{21}$	$2.60^{+0.06}_{-0.04}$	$0.03^{+0.04}_{-0.03}$	$0.17^{+0.02}_{-0.03}$	$6.3^f$	$34^f$	$6.23^f$	1589/1641
$1.85 \pm 0.01$	$(1.89 \pm 0.05) \times 10^{21}$	$2.63^{+0.05}_{-0.06}$	$0.03 \pm 0.03$	$0.29^{+0.04}_{-0.03}$	$6.3^{+4.3}_{-2.6}$	$43^{+16}_{-3}$	$6.22^{+0.05}_{-0.04}$	1542/1637
$1.89 \pm 0.01$	$(1.98^{+0.5}_{-0.6}) \times 10^{21}$	$2.71^{+0.05}_{-0.02}$	$0.10^{+0.03}_{-0.02}$	$0.32^{+0.03}_{-0.04}$	6.2	$44^{+15}_{-2}$	$6.23 \pm 0.04$	2503/2531

Notes:  $^f$  parameter fixed at value

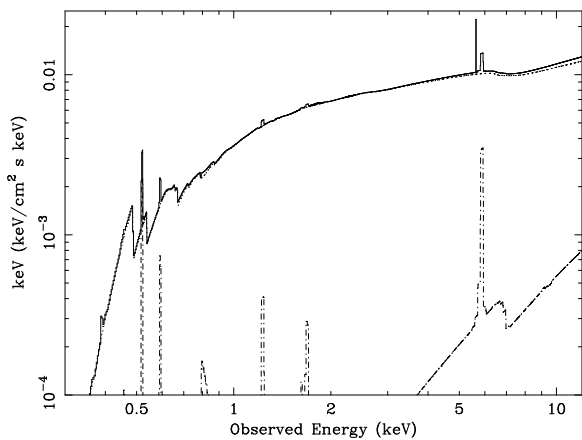


**Figure 4.** The best fitting model to the 0.3–12 keV spectrum of 4C+74.26 (solid line; second line in Table 1). The continuum is comprised of a relativistically blurred ionized reflector (dot-dashed line) and a neutral reflector (dashed line).

'absori' model (the extra cold absorption was still included in the model). To simplify the procedure, the fit was performed with the Fe K $\alpha$  line parameters frozen as in the first line of Table 1. The fit assumed solar abundances and an absorber temperature of  $10^4$  K (higher temperatures did not improve the results). A good fit was obtained ( $\chi^2/\text{d.o.f.}=1616/1641$ ) with a warm absorber column of  $8.8^{+2.4}_{-3.3} \times 10^{20} \text{ cm}^{-2}$  and an ionization parameter of  $56^{+70}_{-44}$ . The intrinsic cold absorption column remained at  $\sim 1.9 \times 10^{21} \text{ cm}^{-2}$ . While this parameterization is clearly inferior compared to a gratings analysis, it is consistent with Kaspi's early inferences of the warm absorber in 4C+74.26.

Using the best-fit model from Table 1, we find a 0.5–2 keV flux of  $8.44 \times 10^{-12} \text{ erg cm}^{-2} \text{ s}^{-1}$  and a 0.5–10 keV flux of  $3.26 \times 10^{-11} \text{ erg cm}^{-2} \text{ s}^{-1}$ . The total unabsorbed luminosity between 0.5 and 2 (10) keV is  $5.81 \times 10^{44}$  ( $1.25 \times 10^{45}$ )  $\text{ergs s}^{-1}$ . Employing the black hole mass estimate of  $\sim 4 \times 10^9 M_{\odot}$  (Woo & Urry 2002), and assuming that the X-ray luminosity is  $\sim 10$  per cent of the bolometric luminosity, then 4C+74.26 has an Eddington ratio of  $\sim 0.04$ .

As a final check on the results, MOS data between 0.3 and 10 keV were added and joint pn-MOS spectral fits were performed. The normalizations of the MOS spectra were allowed to float relative to the pn spectrum to account for any slight calibration errors. Also, a separate photon-index was fit to the MOS data, as it is known that MOS spectra are slightly harder than ones observed from the pn (Vaughan & Fabian 2004). The joint pn-MOS fits re-

sulted in a slightly steeper  $\Gamma$  than previously found, and consequently more absorption in the edges and intrinsic cold absorber was required. The parameter values from our best fit model are shown in the last line in Table 1. One can see there is only minor changes in the fit parameters. When the 'absori' model was used, the warm absorber column reduced to  $7 \times 10^{20} \text{ cm}^{-2}$ , and the ionization parameter also fell to 45. Both these values are well within the errorbars of the previous ones found using only the pn data.

#### 4.1 Partial covering models

Paper I presented evidence for a relativistically broadened Fe K $\alpha$  in the 2–12 keV spectrum of 4C+74.26. The broad line was the statistically preferred fit, but as seen in other AGN (Schurch et al. 2003; Reeves et al. 2004; Gallo et al. 2004; Turner et al. 2005) the breadth of the Fe K $\alpha$  may also be explained by a complicated absorption model. In this section we test if complex absorption models can provide a better fit to the broadband data than one involving a broad Fe K $\alpha$  line.

The pn data are employed between 0.3–12 keV to make use of its superior sensitivity at 6 keV. In contrast to NGC 3783 (Reeves et al. 2004) and NGC 3516 (Turner et al. 2005), 4C+74.26 does not have a very significant warm absorber. The highly ionized component detected by *Chandra* was termed as "weak" (Kaspi, private communication). Furthermore, the column estimated from the 'absori' model is one to two orders of magnitude lower than the columns found in NGC 3783 or NGC 3516. Therefore, it seems unlikely that curvature caused by ionized absorption will significantly effect the spectrum at energies close to the iron line. As a result, we concentrate on partial covering models (Holt et al. 1980) and use the 'zpcfabs' model within XSPEC to simulate the effect of the primary X-ray continuum passing through a neutral absorber with hydrogen column density  $N_{\text{pc}}$  that covers a fraction  $f_{\text{pc}}$  of the X-ray source. The attenuated continuum is assumed to consist of a reflection spectrum, modeled with the 'pexrav' code of Magdziarz & Zdziarski (1995) (same parameter values as in Paper I), and an intrinsically narrow ( $\sigma = 0.01$  keV) neutral Fe K $\alpha$  line. The warm absorber is modeled with the O VII and O VIII edges, and Galactic absorption was also included. The subsequent fit was poor with  $\chi^2/\text{d.o.f.}=1752/1640$ ,  $N_{\text{pc}} \approx 8 \times 10^{20} \text{ cm}^{-2}$ , and  $f_{\text{pc}} = 0.95$ . An improved fit was found by adding additional cold absorption with the 'ztbabs' model. In this case,  $\chi^2/\text{d.o.f.}=1674/1639$ ,  $N_{\text{pc}} \approx 4 \times 10^{22} \text{ cm}^{-2}$  and  $f_{\text{pc}} = 0.25$ . This fit also gave a photon-index of  $\Gamma = 2.1$  and a reflection fraction of 2.5. The column of extra cold absorption was  $1.2 \times 10^{21} \text{ cm}^{-2}$ . A further improvement to  $\chi^2/\text{d.o.f.}=1631/1640$  was found by replacing the 'pexrav'

and Gaussian models with a solar abundance Ross et al. (1999) reflector that had its ionization parameter frozen at its lowest value. In this case,  $N_{\text{pc}} \approx 7 \times 10^{22} \text{ cm}^{-2}$  and  $f_{\text{pc}} = 0.22$ . The photon-index was  $\Gamma = 1.93$  and a low reflection fraction of 0.4 was also found.

In summary, all the partial covering models considered here provide poorer fits to the 0.3–12 keV pn spectrum of 4C+74.26 than the ones that included a relativistically broadened Fe K $\alpha$  line. The line should still be confirmed with a higher signal-to-noise observation, but these results help strengthen the conclusions presented in Paper I.

## 4.2 A spurious high-energy absorption line

Figures 2 and 3 both show a possible absorption line in the residuals at  $\sim 8$  keV. A narrow ( $\sigma = 0$ ) Gaussian absorption line added to the best-fit model described above resulted in a  $\Delta\chi^2 = -10$  with 2 extra degrees of freedom, significant at the 99.5 per cent level according to the F-test. However, this line is not of an astrophysical origin. It arises from the subtraction of a strong Cu K $\alpha$  emission line in the background spectrum produced by the circuit board supporting the pn detector in the spacecraft (Katayama et al. 2004 and references therein). It is important to note that the strength of this line is not constant over the instrument. In fact, it is practically absent near the center where the image of the target source falls. But, if the background accumulation region is closer to the edge of a CCD (as it was in this case), it will include this line which will then produce a spurious absorption feature in the source data. Interestingly, if the line was interpreted as Fe XXVI Ly $\alpha$ , whose rest energy is 6.97 keV, then one would conclude that it was blueshifted to a velocity of  $\sim 0.2c$ . Thus, this feature could easily be misidentified as a highly ionized and rapidly outflowing absorption feature.

As the Cu K $\alpha$  line is very narrow, when our 4C+74.26 spectral analysis was repeated with a different background region that omitted the line, the results did not significantly change. We therefore included the affected plots in this paper to illustrate the potential danger to future authors.

## 5 DISCUSSION

This paper presented the first detailed characterization of the broadband X-ray spectrum of 4C+74.26. At energies less than 2 keV, the spectrum is dominated by cold absorption in excess of the Galactic column in this direction. If this extra attenuation is at the redshift of 4C+74.26, then the column required is  $\sim 1.9 \times 10^{21} \text{ cm}^{-2}$ . This value is about two times smaller than the previous estimates based on either *ASCA* or *BeppoSAX* data (Sambruna et al. 1999; Hasenkopf et al. 2002), although it is not too different from the Reeves & Turner (2000) value. Differing spectral models, analysis techniques and the superior quality of the *XMM-Newton* data are most likely responsible for these disagreements. An excess column of cold absorption appears to be common in radio-loud AGN (Sambruna et al. 1999; Rinn, Sambruna & Gliozzi 2005), and 4C+74.26 is no different despite exhibiting typical Seyfert properties in almost every other regard. In this case, perhaps the larger inclination angle of 35–40 degrees (as inferred from the Fe K $\alpha$  emission line; Paper I & Table 1) implies that the line-of-sight to the central engine has a longer path length within the host galaxy. Alternatively, the host galaxy of 4C+74.26, like most radio-loud AGN, is an elliptical; therefore, unlike spiral galaxies, random

lines-of-sights into the galaxy are unlikely to have a clear path to the center.

In addition to the excess cold absorption, 4C+74.26 also exhibits a weak warm absorber, as primarily evidenced by a significant O VII edge. While a proper parametrization of the warm absorber awaits a long gratings observation, we estimated the absorbing column and ionization parameter to be  $\sim 9 \times 10^{20} \text{ cm}^{-2}$  and  $\sim 60$ , respectively. The high-throughput capabilities of *XMM-Newton* are allowing the discovery of warm absorbers in many more quasars than before (Piconcelli et al. 2005), emphasizing that they are a common occurrence in all accreting supermassive black holes.

This analysis of the soft X-ray spectrum of 4C+74.26 does offer one surprise that will need to be followed up with a longer observation. The best fit broadband spectral model shown in Fig. 4 includes a very weakly ionized reflector which predicts a number of recombination lines at low energies (e.g. Ross et al. 1999), in particular from O VII and O VIII. These lines do seem to fit the data, but whether they originate in the accretion disk or warm absorber (or both) is unknown. This may be elucidated with a long gratings observation of 4C+74.26 which would unravel the properties of the warm absorber.

## ACKNOWLEDGMENTS

Based on observations obtained with *XMM-Newton*, an ESA science mission with instruments and contributions directly funded by ESA Member States and the USA (NASA). The author acknowledges financial support from the Natural Sciences and Engineering Research Council of Canada, and thanks J. Golding for help with the data processing and analysis.

## REFERENCES

- Arnaud K.A., 1996, in Jacoby G.H., Barnes J., eds., ASP Conf. Ser. 101, Astronomical Data Analysis Software and Systems V (Astron. Soc. Pac.: San Francisco), 17
- Ballantyne D.R., Fabian A.C., 2005, ApJ, 622, L97 (Paper I)
- Ballet J., 1999, A&AS, 135, 371
- Brinkmann W., Yuan W., Siebert J., 1997, A&A, 319, 413
- Brinkmann W., Otani C., Wagner S.J., Siebert, J., 1998, A&A, 330, 67
- Corbin M.R., 1997, ApJS, 113, 245
- den Herder J.W. et al., 2001, A&A, 365, L7
- Dickey J.M., Lockman F.J., 1990, ARA&A, 28, 215
- Done C., Mulchaey J.S., Mushotzky R.F., Arnaud K.A., 1992, ApJ, 395, 275
- Gallo L.C., Tanaka Y., Boller Th., Fabian A.C., Vaughan S., Brandt W.N., 2004, MNRAS, 353, 1064
- Hasenkopf C.A., Sambruna R.M., Eracleous M., 2002, ApJ, 575, 127
- Holt S.S., Mushotzky R.F., Boldt E.A., Serlemitsos P.J., Becker R.H., Szymkowiak A.E., White N.E., 1980, ApJ, 241, 13
- Jansen F. et al., 2001, A&A, 365, L1
- Kaspi S., 2004, in Bergmann Th. S., Ho L.C. & Schmitt H.R., eds., IAU Symp. 221, The Interplay Among Black Holes, Stars and ISM in Galactic Nuclei (Cambridge Univ. Press: Cambridge), 41
- Kaspi S., Smith P.S., Netzer H., Maoz D., Jannuzi B.T., Giveon U., 2000, ApJ, 533, 631

- Katayama H., Takahashi I., Ikebe Y., Matsushita K., Freyberg M.J., 2004, *A&A*, 414, 767
- Komossa S., Meerschweinchen J., 2000, *A&A*, 354, 411
- Lara L., Cotton W.D., Feretti L., Giovannini G., Marcaide J.M., Márquez I., Venturi T., 2001, *A&A*, 370, 409
- Lara L., Giovannini G., Cotton W.D., Feretti L., Marcaide J.M., Márquez I., Venturi T., 2004, *A&A*, 421, 899
- Magdziarz P., Zdziarski A.A., 1995, *MNRAS*, 273, 837
- Mason K.O. et al., 2001, *A&A*, 365, L36
- Pearson T.J., Blundell K.M., Riley J.M., Warner P.J., 1992, *MNRAS*, 259, 13p
- Piconcelli E., Jinenez-Bailón E., Guainazzi M., Schartel N., Rodríguez-Pascual P.M., Santos-Lleó M., 2005, *A&A*, 432, 15
- Reeves J.N., Turner M.J.L., 2000, *MNRAS*, 316, 234
- Reeves J.N., Nandra K., George I.M., Pounds K.A., Turner T.J., Yaqoob T., 2004, *ApJ*, 602, 648
- Riley J.M., Warner P.J., 1990, *MNRAS*, 246, 1p
- Riley J.M., Warner P.J., Rawlings S., Saunders R., Pooley G.G., Eales S.A., 1988, *MNRAS*, 236, 13p
- Rinn A.S., Sambruna R.M., Gliozzi M., 2005, *ApJ*, 621, 167
- Robinson A., Corbett E.A., Axon D.J., Young S., 1999, *MNRAS*, 305, 97
- Ross R.R., Fabian A.C., Young A.J., 1999, *MNRAS*, 306, 461
- Sambruna R.M., Eracleous M., Mushotzky, R.F., 1999, *ApJ*, 526, 60
- Schurch N.J., Warwick R.S., Griffiths R.E., Sembay S., 2003, *MNRAS*, 345, 423
- Spergel D.N. et al., 2003, *ApJS*, 148, 175
- Strüder L. et al., 2001, *A&A*, 365, L18
- Turner M.J.L. et al., 2001, *A&A*, 365, L27
- Turner T.J., Kraemer S.B., George I.M., Reeves J.N., Bottorff M.C., 2005, *ApJ*, 618, 155
- Vaughan S., Fabian A.C., 2004, *MNRAS*, 348, 1415
- Wilms J., Allen A., McCray R., 2000, *ApJ*, 542, 914
- Woo J.-H., Urry C.M., 2002, *ApJ*, 579, 530

This paper has been typeset from a  $\text{\TeX}/\text{\LaTeX}$  file prepared by the author.